Turbulent superstructures in Rayleigh-Bénard convection for varying Prandtl numbers

Ambrish Pandey & Jörg Schumacher

Institut für Thermo- und Fluiddynamik
Technische Universität Ilmenau, Germany

June 16, 2017

Outline

Introduction
- Motivation
- Equations
- Simulation Details

Results
- Mean profiles and global transport of heat and momentum
- Instantaneous and time-averaged patterns of velocity and temperature
- Defects in patterns

Conclusions

Outline

Motivation : Solar Granulation and Supergranulation

- $Ra \gtrsim 10^{22}$ and $Pr \lesssim 10^{-3}$
- Granules: a physical pattern covering the surface of the quiet Sun[1]
- Diameter of a typical granule is about $1,000 - 2,000\ km$.
- Supergranules are bigger structures with typical horizontal scale $\sim 30,000\ km$
- Regular patterns at extreme Rayleigh and Prandtl numbers!

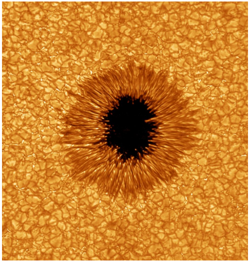

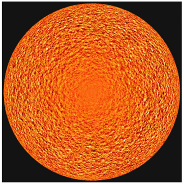

[1] Rieutord and Rincon, Living Rev. Solar Phys., **7** (2010)

Motivation : Solar Granulation and Supergranulation

- $Ra \gtrsim 10^{22}$ and $Pr \lesssim 10^{-3}$
- Granules: a physical pattern covering the surface of the quiet Sun[1]
- Diameter of a typical granule is about $1,000 - 2,000\ km$.
- Supergranules are bigger structures with typical horizontal scale $\sim 30,000\ km$
- Regular patterns at extreme Rayleigh and Prandtl numbers!

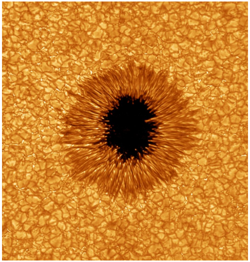

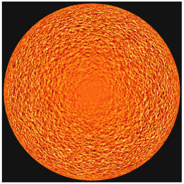

[1] Rieutord and Rincon, Living Rev. Solar Phys., **7** (2010)

Cloud Streets over the Bering Sea (NASA's MODIS Mission)

$Ra \sim 10^{18}$ $\quad$ $Pr \approx 0.7$

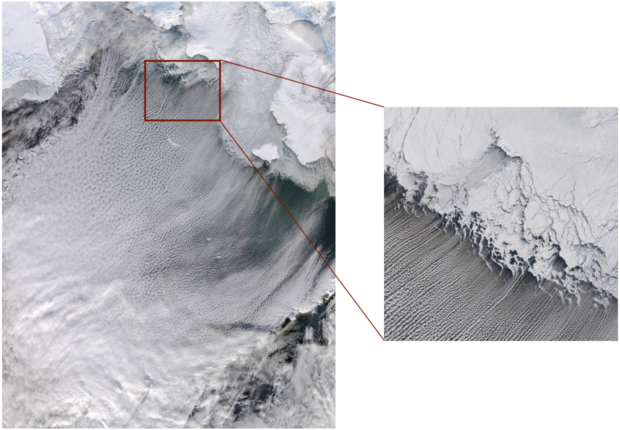

Again! Regular patterns at very high Rayleigh numbers.

Cloud Streets over the Bering Sea (NASA's MODIS Mission)

$Ra \sim 10^{18} \qquad Pr \approx 0.7$

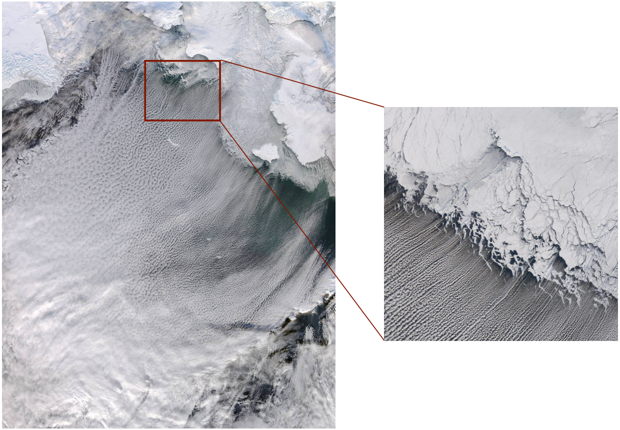

Again! Regular patterns at very high Rayleigh numbers.

Motivation

Patterns are formed in horizontally extended fully turbulent systems, which we will call turbulent superstructures.

- Where do these superstructures come from?
- What is their statistical impact?
- To answer these questions, we study the simplest case of thermal convection: Rayleigh-Bénard convection (RBC).
- A fluid is placed between two horizontal plates, which is heated from below and cooled from above.
- Turbulent transport of heat and momentum depends on fluid parameters and imposed temperature gradient.
- We focus on extended system, in which regular patterns will appear after the turbulent fluctuations are removed (by time-averaging), which are termed as turbulent superstructures.
- Using direct numerical simulations, we characterize their slow dynamics as a function of the Prandtl number.

Motivation

Patterns are formed in horizontally extended fully turbulent systems, which we will call turbulent superstructures.

- Where do these superstructures come from?
- What is their statistical impact?
- To answer these questions, we study the simplest case of thermal convection: Rayleigh-Bénard convection (RBC).
- A fluid is placed between two horizontal plates, which is heated from below and cooled from above.

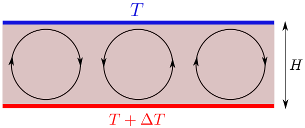

- Turbulent transport of heat and momentum depends on fluid parameters and imposed temperature gradient.
- We focus on extended system, in which regular patterns will appear after the turbulent fluctuations are removed (by time-averaging), which are termed as turbulent superstructures.
- Using direct numerical simulations, we characterize their slow dynamics as a function of the Prandtl number.

Motivation

Patterns are formed in horizontally extended fully turbulent systems, which we will call turbulent superstructures.

- Where do these superstructures come from?
- What is their statistical impact?
- To answer these questions, we study the simplest case of thermal convection: Rayleigh-Bénard convection (RBC).
- A fluid is placed between two horizontal plates, which is heated from below and cooled from above.

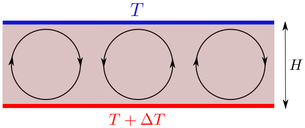

- Turbulent transport of heat and momentum depends on fluid parameters and imposed temperature gradient.
- We focus on extended system, in which regular patterns will appear after the turbulent fluctuations are removed (by time-averaging), which are termed as turbulent superstructures.
- Using direct numerical simulations, we characterize their slow dynamics as a function of the Prandtl number.

Motivation

Patterns are formed in horizontally extended fully turbulent systems, which we will call turbulent superstructures.

- Where do these superstructures come from?
- What is their statistical impact?
- To answer these questions, we study the simplest case of thermal convection: Rayleigh-Bénard convection (RBC).
- A fluid is placed between two horizontal plates, which is heated from below and cooled from above.

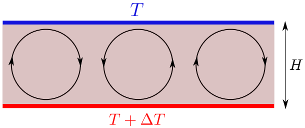

- Turbulent transport of heat and momentum depends on fluid parameters and imposed temperature gradient.
- We focus on extended system, in which regular patterns will appear after the turbulent fluctuations are removed (by time-averaging), which are termed as turbulent superstructures.
- Using direct numerical simulations, we characterize their slow dynamics as a function of the Prandtl number.

Motivation

Patterns are formed in horizontally extended fully turbulent systems, which we will call turbulent superstructures.

- Where do these superstructures come from?
- What is their statistical impact?
- To answer these questions, we study the simplest case of thermal convection: Rayleigh-Bénard convection (RBC).
- A fluid is placed between two horizontal plates, which is heated from below and cooled from above.

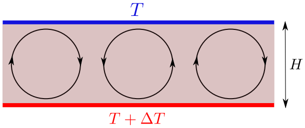

- Turbulent transport of heat and momentum depends on fluid parameters and imposed temperature gradient.
- We focus on extended system, in which regular patterns will appear after the turbulent fluctuations are removed (by time-averaging), which are termed as turbulent superstructures.
- Using direct numerical simulations, we characterize their slow dynamics as a function of the Prandtl number.

Governing equations

Conservation of mass, momentum, and internal energy leads to governing equations of RBC.
Under Boussinesq approximations, these equations are:

$$
\begin{aligned}
\frac{\partial \mathbf{u}}{\partial t} + \mathbf{u}\cdot\nabla\mathbf{u} &= -\frac{\nabla p}{\rho_0} + \alpha g(T - T_0)\hat{z} + \nu\nabla^2\mathbf{u}, \\
\frac{\partial T}{\partial t} + \mathbf{u}\cdot\nabla T &= \kappa\nabla^2 T, \\
\nabla\cdot\mathbf{u} &= 0
\end{aligned}
$$

$\mathbf{u}(x,y,z)$: velocity field
$T(x,y,z)$: temperature field
$p(x,y,z)$: pressure field

g : acceleration due to gravity
ν : kinematic viscosity
κ : thermal diffusivity

Important parameters

$Ra = \frac{\alpha g(\Delta T)H^3}{\nu\kappa}$ $\quad Pr = \frac{\nu}{\kappa}$ $\quad \Gamma = \frac{L}{H}$

Governing equations

Conservation of mass, momentum, and internal energy leads to governing equations of RBC.
Under Boussinesq approximations, these equations are:

$$
\begin{aligned}
\frac{\partial \mathbf{u}}{\partial t} + \mathbf{u} \cdot \nabla \mathbf{u} &= -\frac{\nabla p}{\rho_0} + \alpha g (T - T_0)\hat{z} + \nu \nabla^2 \mathbf{u}, \\
\frac{\partial T}{\partial t} + \mathbf{u} \cdot \nabla T &= \kappa \nabla^2 T, \\
\nabla \cdot \mathbf{u} &= 0
\end{aligned}
$$

$\mathbf{u}(x, y, z)$: velocity field
$T(x, y, z)$: temperature field
$p(x, y, z)$: pressure field

g : acceleration due to gravity
ν : kinematic viscosity
κ : thermal diffusivity

Important parameters

$Ra = \frac{\alpha g (\Delta T) H^3}{\nu \kappa}$ $\quad$ $Pr = \frac{\nu}{\kappa}$ $\quad$ $\Gamma = \frac{L}{H}$

Simulation details

- Geometry : Rectangular box of dimensions 25 : 25 : 1
- Velocity BC : No-slip at all the walls
- Temperature BC : Isothermal at top and bottom; adiabatic on sidewalls
- Numerical method : Spectral element solver NEK5000[2,3]
- $Pr = 0.021$ (mercury), 0.7 (air), 7.0 (water) & $Ra = 10^5$

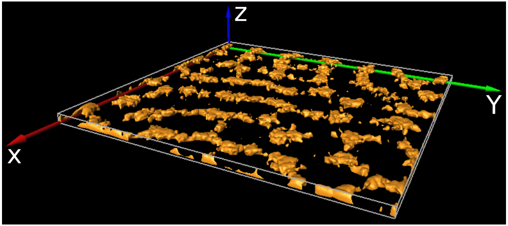

Figure: Isosurfaces of $\langle u_z T \rangle_{t=0.5t_d}$ for $Pr = 0.7$. Structures are moving upward.

[2] Fischer, J. Comp. Phys. **133** (1997)
[3] Scheel, Emran, and Schumacher, New J. Phys. **15** (2013)

Outline

Temperature and velocity profiles

Horizontally-averaged temperature $\langle T \rangle_{A,t}$ and rms horizontal velocity $U_{\mathrm{rms}} = \sqrt{\langle u_x^2 + u_y^2 \rangle_{A,t}}$ vary strongly near the top and bottom plates.

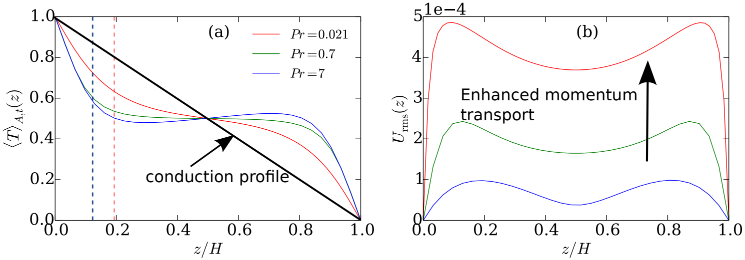

Figure: Dashed lines represent thermal boundary thicknesses.

For $Pr = 7$, $\langle T \rangle_{A,t}$ exhibits positive gradient in the bulk, possibly due to plume overshoot.

Nondimensional heat and momentum transfer

Nusselt number (*Nu*): A measure of the turbulent heat transfer

$$
\begin{aligned}
Nu(z) &= \frac{\langle u_z T\rangle_{A,t} - \kappa \frac{\partial \langle T\rangle_{A,t}}{\partial z}}{\kappa \frac{\Delta T}{H}} = \text{const}, \\
Nu &= 1 + \frac{H}{\kappa \Delta T} \langle u_z T\rangle_{V,t}
\end{aligned}
$$

Reynolds number (*Re*): A measure of the turbulent momentum transfer

$$Re = \frac{UH}{\nu},$$

where

$$U = \sqrt{\langle u_i^2\rangle_{V,t}}$$

$Nu \sim Ra^{\alpha} Pr^{\beta}, \alpha \approx 0.25 - 0.33$ $\qquad$ $Re \sim Ra^{\gamma} Pr^{\zeta}, \gamma \approx 0.42 - 0.60$

Nondimensional heat and momentum transfer

Nusselt number (*Nu*): A measure of the turbulent heat transfer

$$Nu(z) = \frac{\langle u_z T\rangle_{A,t} - \kappa \frac{\partial \langle T\rangle_{A,t}}{\partial z}}{\kappa \frac{\Delta T}{H}} = \mathrm{const},$$

$$Nu = 1 + \frac{H}{\kappa \Delta T} \langle u_z T\rangle_{V,t}$$

Reynolds number (*Re*): A measure of the turbulent momentum transfer

$$Re = \frac{UH}{\nu},$$

where

$$U = \sqrt{\langle u_i^2\rangle_{V,t}}$$

$$Nu \sim Ra^{\alpha} Pr^{\beta}, \alpha \approx 0.25 - 0.33 \qquad Re \sim Ra^{\gamma} Pr^{\zeta}, \gamma \approx 0.42 - 0.60$$

Turbulent transport

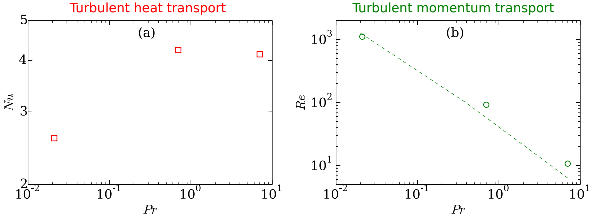

Dashed curve: fit from the model of Pandey and Verma (POF 2016, PRE 2016)

$$Re = \frac{-c_4 + \sqrt{c_4^2 + 4(c_1 - c_2)c_3 Ra/Pr}}{2(c_1 - c_2)}$$

The coefficients $c_i(Ra, Pr)$ have been determined using simulation data.

$Nu(Pr)$ and $Re(Pr)$ are also consistent with the predictions of GL theory[4].

[4] Grossmann and Lohse, J. Fluid Mech. **407** (2000)

Turbulent transport

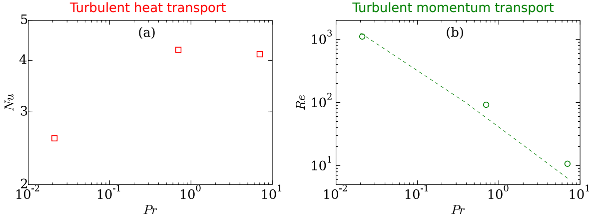

Dashed curve: fit from the model of Pandey and Verma (POF 2016, PRE 2016)

$$Re = \frac{-c_4 + \sqrt{c_4^2 + 4(c_1 - c_2)c_3 Ra/Pr}}{2(c_1 - c_2)}$$

The coefficients $c_i(Ra, Pr)$ have been determined using simulation data.

$Nu(Pr)$ and $Re(Pr)$ are also consistent with the predictions of GL theory[4].

[4] Grossmann and Lohse, J. Fluid Mech. **407** (2000)

Turbulent transport

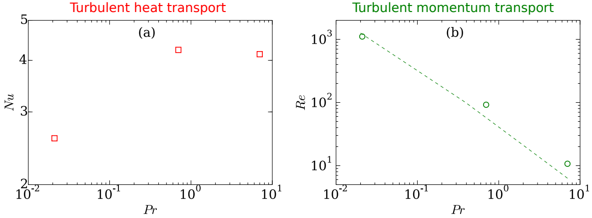

Dashed curve: fit from the model of Pandey and Verma (POF 2016, PRE 2016)

$$Re = \frac{-c_4 + \sqrt{c_4^2 + 4(c_1 - c_2)c_3 Ra/Pr}}{2(c_1 - c_2)}$$

The coefficients $c_i(Ra, Pr)$ have been determined using simulation data.

$Nu(Pr)$ and $Re(Pr)$ are also consistent with the predictions of GL theory[4].

[4] Grossmann and Lohse, J. Fluid Mech. **407** (2000)

Time-scales in RBC

- Free-fall time $t_f = \frac{H}{u_f} = \frac{H}{\sqrt{\alpha g (\Delta T) H}}$
- Diffusion time $t_d = \frac{H^2}{\kappa} = \sqrt{RaPr}\, t_f$
- Viscous time $t_v = \frac{H^2}{\nu} = \sqrt{\frac{Ra}{Pr}}\, t_f$
- Plume detachment time scale[5] $\sim t_f$
- Lagrangian eddy turnover time[6] $\sim 10 t_f$

Table: Typical diffusion time scales for $Ra = 10^5$

Pr	t_f	t_d	t_v
0.021	1.0	45.8	2182
0.7	1.0	264.6	378.0
7	1.0	836.6	119.5

In the following we study dynamics in units of the vertical diffusion time.

[5] Shi, Emran and Schumacher, J. Fluid Mech. **706** (2012)
[6] Emran and Schumacher, Phys. Rev. E **82** (2010)

Time-scales in RBC

- Free-fall time $t_f = \frac{H}{u_f} = \frac{H}{\sqrt{\alpha g(\Delta T)H}}$
- Diffusion time $t_d = \frac{H^2}{\kappa} = \sqrt{RaPr}\,t_f$
- Viscous time $t_v = \frac{H^2}{\nu} = \sqrt{\frac{Ra}{Pr}}\,t_f$
- Plume detachment time scale[5] $\sim t_f$
- Lagrangian eddy turnover time[6] $\sim 10t_f$

Table: Typical diffusion time scales for $Ra = 10^5$

Pr	t_f	t_d	t_v
0.021	1.0	45.8	2182
0.7	1.0	264.6	378.0
7	1.0	836.6	119.5

In the following we study dynamics in units of the vertical diffusion time.

[5] Shi, Emran and Schumacher, J. Fluid Mech. **706** (2012)

[6] Emran and Schumacher, Phys. Rev. E **82** (2010)

Temperature field in mid-horizontal plane

$\langle T(x, y, z = H/2) \rangle_t$ for $Pr = 0.7$
Averaging interval centered around the instantaneous snapshot.

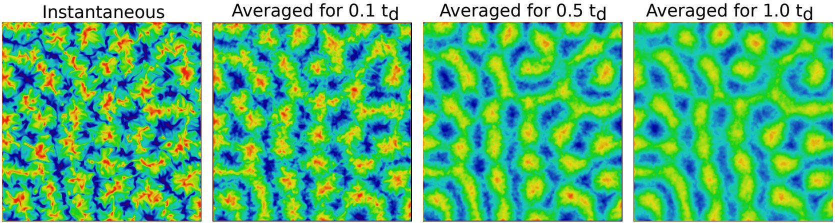

Averaging should be long enough for patters to appear.

Should not be too long to wash out all patterns.

We find that $t = 0.5t_d$ is the appropriate time scale for subsequent analysis.

Temperature field in mid-horizontal plane

$\langle T(x, y, z = H/2) \rangle_t$ for $Pr = 0.7$
Averaging interval centered around the instantaneous snapshot.

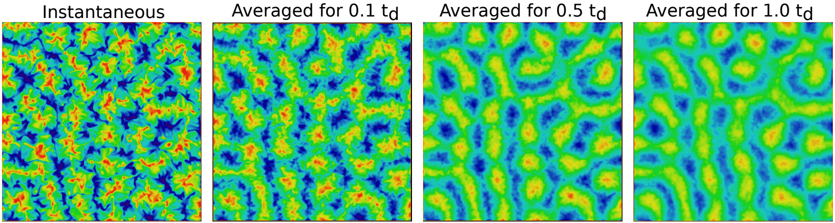

Averaging should be long enough for patters to appear.

Should not be too long to wash out all patterns.

We find that $t = 0.5 t_d$ is the appropriate time scale for subsequent analysis.

Velocity streamlines and temperature contours for time-averaged field

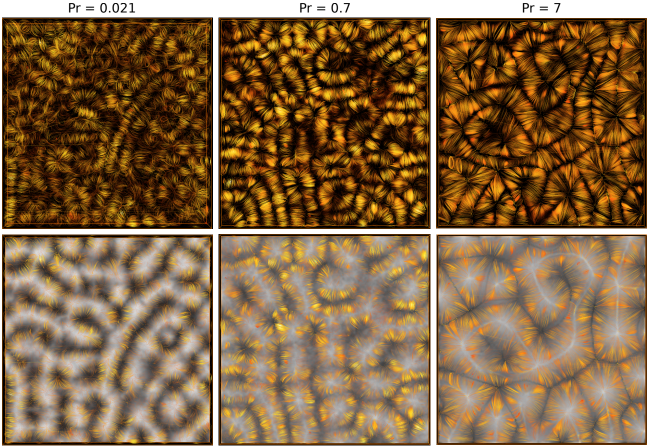

Regular pattern for all Prandtl numbers!

Vertical velocity field and its Fourier transform

$$\langle u_z(x, y, z = H/2) \rangle_{t=0.5t_d}$$

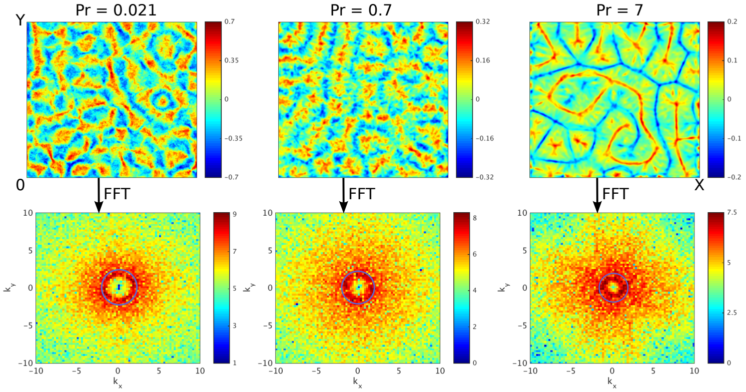

Characteristic scales grow with increasing *Pr*.

Vertical velocity field and its Fourier transform

$$\langle u_z(x, y, z = H/2) \rangle_{t=0.5t_d}$$

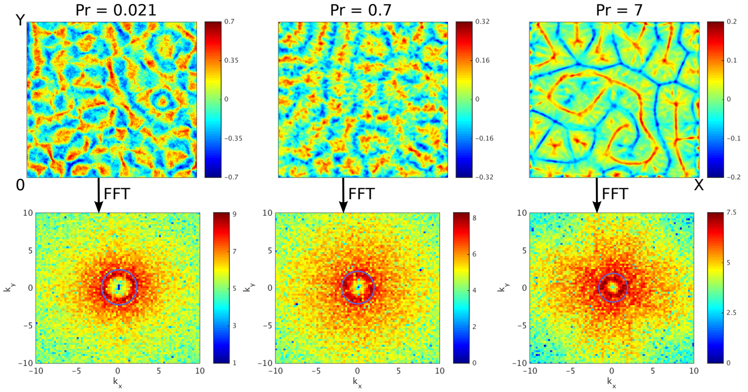

Characteristic scales grow with increasing *Pr*.

Time-averaged correlation functions

$$u_z(x,y,z) = \langle u_z(x,y,z=H/2)\rangle_{t=0.5t_d} \qquad \theta(x,y,z) = \langle \theta(x,y,z=H/2)\rangle_{t=0.5t_d}$$

$$C^x_{u_z}(r) = \frac{\langle u_z(x+r,y,z)u_z(x,y,z)\rangle_{A,z=H/2}}{\langle u_z^2(x,y,z)\rangle_{A,z=H/2}} \qquad C^x_{\theta}(r) = \frac{\langle \theta(x+r,y,z)\theta(x,y,z)\rangle_{A,z=H/2}}{\langle \theta^2(x,y,z)\rangle_{A,z=H/2}}$$

$$C^y_{u_z}(r) = \frac{\langle u_z(x,y+r,z)u_z(x,y,z)\rangle_{A,z=H/2}}{\langle u_z^2(x,y,z)\rangle_{A,z=H/2}} \qquad C^y_{\theta}(r) = \frac{\langle \theta(x,y+r,z)\theta(x,y,z)\rangle_{A,z=H/2}}{\langle \theta^2(x,y,z)\rangle_{A,z=H/2}}$$

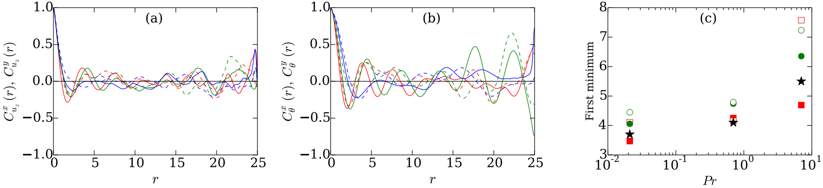

Figure: Solid curves: $C^x(r)$. Dashed curves: $C^y(r)$

Again scales grow with increasing *Pr*.

Time-averaged correlation functions

$$u_z(x,y,z) = \langle u_z(x,y,z=H/2)\rangle_{t=0.5t_d} \qquad \theta(x,y,z) = \langle \theta(x,y,z=H/2)\rangle_{t=0.5t_d}$$

$$C^x_{u_z}(r) = \frac{\langle u_z(x+r,y,z)u_z(x,y,z)\rangle_{A,z=H/2}}{\langle u_z^2(x,y,z)\rangle_{A,z=H/2}} \qquad C^x_{\theta}(r) = \frac{\langle \theta(x+r,y,z)\theta(x,y,z)\rangle_{A,z=H/2}}{\langle \theta^2(x,y,z)\rangle_{A,z=H/2}}$$

$$C^y_{u_z}(r) = \frac{\langle u_z(x,y+r,z)u_z(x,y,z)\rangle_{A,z=H/2}}{\langle u_z^2(x,y,z)\rangle_{A,z=H/2}} \qquad C^y_{\theta}(r) = \frac{\langle \theta(x,y+r,z)\theta(x,y,z)\rangle_{A,z=H/2}}{\langle \theta^2(x,y,z)\rangle_{A,z=H/2}}$$

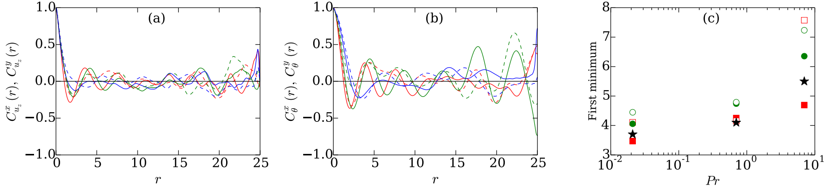

Figure: Solid curves: $C^x(r)$. Dashed curves: $C^y(r)$

Again scales grow with increasing *Pr*.

Defects in patterns

Morris et al.[7] observed defects[8] in $\Gamma = 78$ cell near the onset of convection ($\Delta T = 1.116 \Delta T_c$).

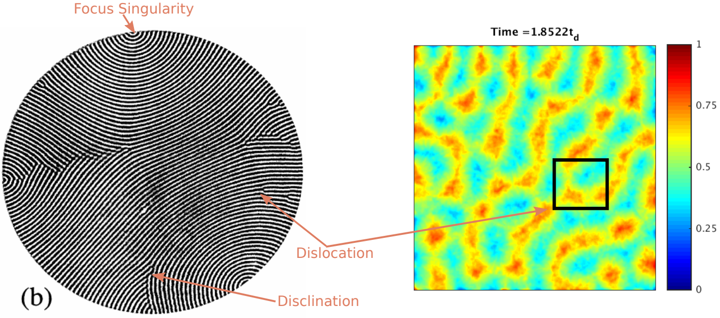

We also detect defects in the time-averaged temperature field.

[7] Morris et al., Phys. Rev. Lett. **77** (1993)
[8] Bodenschatz et al., Annu. Rev. Fluid Mech. **32** (2000)

Sliding average of temperature field

Each frame in movies is averaged for half a thermal diffusion time.

$Pr = 0.021$ $Pr = 0.7$ $Pr = 7$

- Defects are detected for all Prandtl numbers.
- Pattern evolves by annihilation and creation of defects.

Movement of defects for $Pr = 0.7$

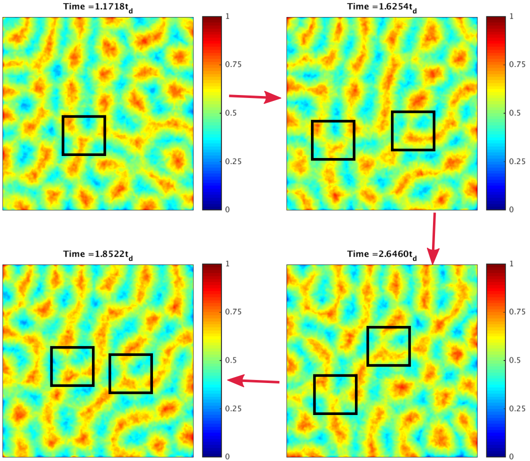

Patterns evolve on a slow time scale of the order of the diffusion time.

Outline

Summary

- We study the characteristics of turbulent superstructures in a large aspect ratio RBC.
- Performed long-term DNS for $Pr = 0.021, 0.7, 7$ and $Ra = 10^5$ for more than three vertical diffusion times.
- Pr-dependence of Nu and Re is consistent with results for $\Gamma \approx 1$ RBC.

- Time-averaged fields reveal patterns similar to those for lower Ra.
- Characteristic length scale of these patterns is determined in Fourier space, and consistent with correlation scale in physical space.
- Typical pattern scale increases with increasing Prandtl number at fixed Ra.

- Defects in the time-averaged patterns are detected for all the Prandtl numbers.
- The defects are annihilated and created on the order of a thermal diffusion time.

- We are continuing our analysis for larger Rayleigh numbers and smaller Prandtl numbers ($Pr = 0.005$).
- We also started to analyze superstructures in the Lagrangian frame of reference by spectral graph clustering.

Summary

- We study the characteristics of turbulent superstructures in a large aspect ratio RBC.
- Performed long-term DNS for $Pr = 0.021, 0.7, 7$ and $Ra = 10^5$ for more than three vertical diffusion times.
- Pr-dependence of Nu and Re is consistent with results for $\Gamma \approx 1$ RBC.

- Time-averaged fields reveal patterns similar to those for lower Ra.
- Characteristic length scale of these patterns is determined in Fourier space, and consistent with correlation scale in physical space.
- Typical pattern scale increases with increasing Prandtl number at fixed Ra.

- Defects in the time-averaged patterns are detected for all the Prandtl numbers.
- The defects are annihilated and created on the order of a thermal diffusion time.

- We are continuing our analysis for larger Rayleigh numbers and smaller Prandtl numbers ($Pr = 0.005$).
- We also started to analyze superstructures in the Lagrangian frame of reference by spectral graph clustering.

Summary

- We study the characteristics of turbulent superstructures in a large aspect ratio RBC.
- Performed long-term DNS for $Pr = 0.021, 0.7, 7$ and $Ra = 10^5$ for more than three vertical diffusion times.
- *Pr*-dependence of *Nu* and *Re* is consistent with results for $\Gamma \approx 1$ RBC.

- Time-averaged fields reveal patterns similar to those for lower *Ra*.
- Characteristic length scale of these patterns is determined in Fourier space, and consistent with correlation scale in physical space.
- Typical pattern scale increases with increasing Prandtl number at fixed *Ra*.

- Defects in the time-averaged patterns are detected for all the Prandtl numbers.
- The defects are annihilated and created on the order of a thermal diffusion time.

- We are continuing our analysis for larger Rayleigh numbers and smaller Prandtl numbers ($Pr = 0.005$).
- We also started to analyze superstructures in the Lagrangian frame of reference by spectral graph clustering.

Summary

- We study the characteristics of turbulent superstructures in a large aspect ratio RBC.
- Performed long-term DNS for $Pr = 0.021, 0.7, 7$ and $Ra = 10^5$ for more than three vertical diffusion times.
- Pr-dependence of Nu and Re is consistent with results for $\Gamma \approx 1$ RBC.

- Time-averaged fields reveal patterns similar to those for lower Ra.
- Characteristic length scale of these patterns is determined in Fourier space, and consistent with correlation scale in physical space.
- Typical pattern scale increases with increasing Prandtl number at fixed Ra.

- Defects in the time-averaged patterns are detected for all the Prandtl numbers.
- The defects are annihilated and created on the order of a thermal diffusion time.

- We are continuing our analysis for larger Rayleigh numbers and smaller Prandtl numbers ($Pr = 0.005$).
- We also started to analyze superstructures in the Lagrangian frame of reference by spectral graph clustering.

Acknowledgement

Computational resources:

lrz Leibniz Supercomputing Centre
of the Bavarian Academy of Sciences and Humanities

GCS
Gauss Centre for Supercomputing

Large scale project 2017/18.

Financial support: Priority program 1881 on Turbulent Superstructures

DFG
Turbulent Superstructures

Thank You
for your attention!

Acknowledgement

Computational resources:

lrz Leibniz Supercomputing Centre of the Bavarian Academy of Sciences and Humanities

GCS Gauss Centre for Supercomputing

Large scale project 2017/18.

Financial support: Priority program 1881 on Turbulent Superstructures

DFG Turbulent Superstructures

Thank You

for your attention!